Original scientific paper

Numerical Analysis of Seismic Behavior of an Arched-Roof 3D-Printed Building

Peyman Narjabadifam[1)], Somayeh Mollaei[*1)], Ehsan Noroozinejad Farsangi[*2)], Yahya Talebi Somahe[1)]

[1)] University of Bonab, Department of Civil Engineering, Velayat Highway, Bonab, East Azerbaijan, Iran
[2)] Urban Transformations Research Centre (UTRC), Western Sydney University, NSW, Australia

ABSTRACT

3D-Printed Concrete (3DPC) can reduce the consumption of materials, construction costs, and implementation time, as well as increase sustainability. Seismic safety is one of the necessities of any structure in a high earthquake hazard zone. The lack of scientific and engineering studies in this area would highlight the importance of studying seismic safety in 3DPC building structures. This paper is focused on the basic specifications of 3DPC buildings under earthquake excitations. The authors conducted a thorough theoretical study due to the pilot nature of the research. A prescriptive evaluation was conducted based on the existing seismic regulations for similar structures. The main goal of the research was to create the necessary platform for applied studies, which was achieved through theoretical investigations and prescriptive evaluations. For this purpose, the finite element modeling of a 3DPC building with an arch roofing system was implemented and analyzed using ABAQUS software. Based on the main results, the most remarkable weakness of such a structure was the material's poor tension behavior. The arrangement of the internal partitions (infill walls), the shear performance of the walls, and the relative displacement of the components were other effective factors of the 3DPC building under seismic loads. The results showed that the truss-like performance of the arch roof in the considered 3DPC building probably caused the undesirable structural responses under the seismic loads.

1 Introduction

Using 3D-Printed Concrete (3DPC) in buildings can reduce the use of materials, costs, and construction time and increase the sustainability of the building. This technology has other futuristic advantages, such as the ease of transferring the building even to other planets [1-3]. Due to the on-site construction and use of local materials, 3D printing of the buildings significantly reduces transportation costs [4]. This method also substantially reduces adverse environmental effects such as high energy use, greenhouse gas emissions, water use, and waste production in the construction process [5]. The other significant advantage of this technology is the construction of structures with free forms, which requires complex, heavy, and expensive molding systems in ordinary construction methods [6, 7].

Contour Crafting (CC) technology was developed for the first time by Khoshnevis [8], which was among the first examples of 3D printing using concrete materials. 3D printing technology is a set of sciences that includes the disciplines of material, architectural, structural, mechanical, and software engineering and was created to print structures and pieces on a real scale [9]. 3D printing technology is used in most industries, including aerospace, automotive, medicine, weaponry, and the construction industry [10].

Concrete is the most popular material used in 3D-printed buildings. The essential characteristics of concrete materials used in 3D printing construction include the rheological or fresh properties as well as the hardened properties of the concrete [11, 12]. Most of the materials used in the 3DPC mixture are locally available materials, and the desired properties are achieved by chemical additives. However, most common mortars in 3D-printed buildings consist of microsilica, ordinary Portland cement, fly ash, river sand (up to 2 mm grain size), and polypropylene microfibers [4].

In previous studies, factors affecting the rheological properties of the printed concrete material have been studied, such as time interval, extrusion rate, layer thickness, material composition, fibers, nozzle tip geometry, etc., [3, 6, 7, 12, 13, 14]. Ahmed Saleh [3] evaluated the feasibility of concrete in 3D printing construction. He concluded that 3D concrete printing has a promising future in construction. Jeong et al. [6] proposed a model to derive the rheological properties of the 3D-printed concrete material. It was proven that using sisal fibers in printed mortar led to a higher yield stress and cohesiveness of the mix [7]. Bukvić et al. [12] reviewed the pumpability and printability properties of fresh printable concrete in past research.

---

* Corresponding author:
  E-mail address: s.mollaei@ubonab.ac.ir&ehsan.noroozinejad@westernsydney.edu.au

Khoshnevis [8] reviewed the basic concepts in the construction of a 3D-printed building. The study results showed that the increasing voids in the layers, the lightness of the material, as well as the use of a layered dome form inspired by traditional methods in the bed of modern materials,could be helpful in practical applications [8]. Van et al. [13] studied the interlayer bonding in printed construction. They found that the application of a robust system for 3D concrete printing was as vital as the material properties [13]. Also, Bos et al. [15] conducted a study to reinforce printed concrete using steel cables. They showed that steel reinforcement was a feasible method to achieve improved material behavior.

Martens et al. [16] conducted a study to optimize the material mixture and topology of the structure for 3D-printed buildings. Also, Hojati et al. [17] conducted studies on different mixtures of printed materials, including native materials on Mars. Their studies showed that native materials on Mars have a high potential for printing buildings there. Also, using long fibers can increase the structure's efficiency [17]. Daniel et al. [18] studied the possibility of improving the strength of layers. Their studies showed that shorter time intervals and increased contact area were helpful in improving interlayer bonding [18]. Skibicki et al. [19] tested some novel compositions for printed building materials at different temperatures. Their proposed methods had enhancing effects on the curing time of the printed materials and led to a higher speed of the construction process. Padnis and Shariff [20] proposed a numerical method to calculate the critical buckling height of the 3D-printed walls. They validated the proposed method using test results. Li et al. [14] reviewed the experimental testing on the fresh-state and hardened properties of the materials in 3D-printed concrete.

Pudjisuryadi et al. [1] studied the weaknesses of printed structural beams. They concluded that the use of small-scale samples may not be suitable to predict the behavior of the printed structures. Federowicz et al. [21] investigated the shrinkage of 3D-printed cement materials and the deformations caused by this shrinkage at different time intervals. They showed that the application of anti-shrinkage admixtures did not change the compressive strength of the hardened material. Olobokola [22] investigated the difference between the results of finite element analysis (FEA) and analytical models for 3D-printed components. The study showed a close correlation between manual calculations and computer analyses. Pekuss et al. [23] studied 3D-printed columns with different geometrical complexities. Wang et al. [24] studied the interface properties of the printed concrete layers. The ultimate tensile strength and shear strength of 3D-printed concrete were increased by using steel rebars and fiber reinforcement in the printed material.

Chang et al. [25] proposed a model with a new failure criterion for numerical modeling of 3D-printed concrete. Licciardello et al. [26] conducted experimental studies on the hardening behavior of printed concrete walls. Gebhard et al. [11] investigated the bending behavior of printed beams. Duarte et al. [27] investigated the geometric form of printed buildings. They showed that load-bearing wall systems with shell and arch forms were desirable geometries [27]. Pan et al. [28] investigated the effects of raw material properties on the interlayer bond of printed concrete at different time intervals. Xiao et al. [29] proposed the idea of using recycled materials in 3D-printed buildings.

Recently, Xiao et al. [30] reviewed the literature on appropriate geometric forms and structures for 3DPC buildings. Essebyty et al. [31] investigated the sustainability of 3D-printed buildings in a case study. They showed that the seismic performance of the building was similar to that of an unreinforced masonry building. In another study, Zhang et al. [32] investigated the 3D-printed walls under Gaussian-static loading conditions. Their study proved that the 3DCP building reinforced with FRP textile had desirable mechanical properties. One study on the structural design of printed buildings subject to dynamic loadings is that by Aghajani Delavar et al. [33], who studied the design, modeling, and analysis of 3D-printed walls under dynamic horizontal loads. They proposed analytical equations to forecast the behavior of 3D-printed walls under in-plane seismic loading, which OpenSees numerical results validated.

Reviewing the literature on 3DPC buildings proved that the seismic performance and nonlinear behavior of those buildings have not been widely studied. Most previous studies in this field have focused on the mixture plans and construction methods of 3DPC structures. While seismic safety is one of the basic needs of any structure located in an earthquake-prone environment, printed structures are no exception to this.

Investigating the seismic safety of 3D-printed buildings could be helpful to expand the practical applications of those structures. This issue was considered in this study. This research attempted to determine the basic needs and characteristics of earthquake engineering in 3D-printed structures. Here, defining a prescriptive evaluation process for the seismic safety of printed structures and providing a practical model for a detailed evaluation of the seismic safety of these structures were pursued. For this purpose, an extensive theoretical study was conducted using technical literature related to printed structures. In the following, the existing seismic regulations were used for loading, analysis, and modeling of the considered 3DPC building. Then, a practical phenomenological model was proposed for a 3D-printed structure using ABAQUS finite element software.

2 Materials and methods

The initial hypothesis in this study was that the basic needs of earthquake engineering in printed structures mainly include control of accelerations. Also, another hypothesis of the authors was that a prescriptive evaluation process of printed buildings can be defined based on the existing building seismic criteria. The research process and results are described and discussed in the following parts.

2.1 3D-printed structure considered in the study

As shown in Figure 1a, the considered model was a barrel vault structure with dimensions of 10 × 6 m and a wall height of 3 m with an arch roofing form. The geometric and material properties of the considered building were selected with minimum discontinuity. Therefore, any reinforcements or different material types were not taken into account. The existing 3D printing technologies can guarantee the implementation of the whole building, from the foundation to the rooftop, without human intervention. Hence, the considered 3D-printed structure can be implemented without any human intervention and in all directions, even on other planets. According to previous studies, the arching system is one of the recommended forms for 3D-printed structures [8, 27]. As shown in Figure 1b, on each of the longitudinal perimeter walls (y direction), two openings were considered as windows, and one opening was created as a door at the

transverse end of the building. Also, two inner infill walls were modeled in the considered building. The layers of the walls and roof of the model had a truss-like structure with a 20 cm width. As shown in Figures 1c to 1e, the cross-section of the walls and arch was a two-row truss-like form with a width of 6cm in each row and a distance of 8 cm from each other. The rows were connected by zigzagged grids with a width of 2.5 cm. A cross-section with parallel filaments and a grid pattern between them is widely used for 3D-printed structures [34]. The thickness of every printing layer was assumed to be 4 cm. The specific weight of the printing concrete was 2100 kg/cm³.

The maximum height of the arch at the highest point was 3 m. The dimensions of the foundation were 10 × 6 m, with a thickness of 30 cm. The 3D-printed perimeter walls were assumed to be the lateral and gravitational load-bearing systems of the studied structure. Also, it was assumed that 3D printing technology without human intervention was used in the construction process. Therefore, all the rheological properties of the concrete material were assumed to be isotropic and homogenous. During the construction of the structure, no additional stresses had been applied to the structure due to the movement of the nozzle or its vibrations, so no stress reduction had been considered in the material model.

2.2   Loading of the structure

The regulations used in this study included National Building Regulations of Iran parts 6, 8, and 9 [35-37], which are dedicated to seismic loading and the design and execution requirements of masonry and reinforced concrete buildings, respectively. Also, the Organization of Strategic Planning and Supervision of Iran publications No. 740 and 360 [38, 39] were used in this study, which includes guidelines for seismic evaluation and rehabilitation of buildings. It should be noted that the lack of specialized regulations was the most essential and fundamental limitation of this study. Also, the lack of previous studies on the behavior of 3D-printed structures under the conditions of natural disasters was another limitation.

Here, a residential building was investigated, which was located in Tabriz city, Iran, and on the third soil type. Therefore, according to Iranian seismic standard criteria No. 2800 [40], its experimental period of vibration can be obtained using Equation 1. Based on the mentioned criteria, the equivalent lateral force is the most commonly used technique for seismic analysis.

$$T = 0.08H^{0.75} \tag{1}$$

(a)

(b)

(c)

(d)

(e)

(f)
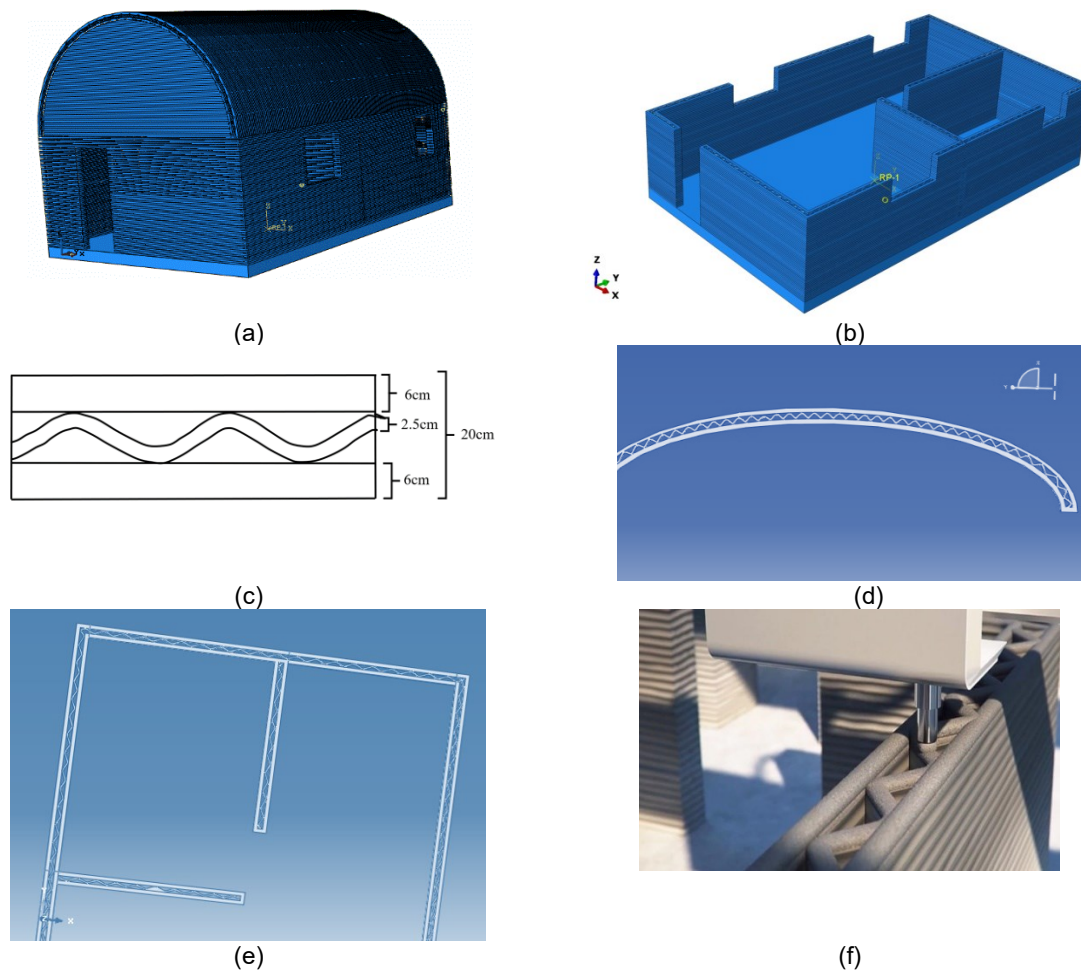
Figure 1. Finite element model of the considered building in this study: a)3D-printed building; b) building plan; c) cross-section of the arch and walls; d) a layer of the modeled arch roof; e) a layer of the modeled walls; f) schematic printing process of the parallel filament with internal grids

Where T is the main period of vibration(s), and H is the height of the building (m).

The reflection coefficient of the building is a parameter that is used for calculating the seismic coefficient of the building, and it can be calculated by Equation (2).

$$B = B_1 N \tag{2}$$

Where B_1 is the spectral shape factor (SSF) and N is the spectral correction factor. B_1 is also calculated by Equation (3).

$$B_1 = \begin{cases} S_o + (S - S_o + 1)\left(\frac{T}{T_o}\right); & 0 < T < T_o \\ S + 1 \; ; & T_o < T < T_o \\ (S + 1)\left(\frac{T}{T_o}\right); & T > T_O \end{cases} \tag{3}$$

Where T is the main period of the building (s), and T_o, T_s, S, and S_o are parameters that depend on the soil type and the seismic zone of the region.

Considering that 3D-printed buildings are not part of any structural systems classified in the existing seismic regulations, and given that this research is a pilot study, the behavior factor of R can be considered equal to 1. This is a conservative assumption.

Given the values of A, B, and R, the seismic coefficient of the building can be obtained from Equation (4).

$$C = ABI/R \tag{4}$$

Where A is the design acceleration, B is the reflection coefficient, I is the importance coefficient, and R is the coefficient of the behavior of the building. The seismic characteristics of the considered building are tabulated in Table 1.

Table 1. Seismic characteristics of the building (based on the regulations [38-40])

A	B	I	R	C	W
0.35	2.75	1	1	0.9625	$55784 kg$

Snow loading, as a live load on the arched roof, was calculated according to the National Building Regulations of Iran Part 6 [33] by Equation (5).

$$Pr = 0.7 Cs Ct Ce IPg \tag{5}$$

Where Pr is the snow load on the arch per square centimeter of the horizontal projection of the surface, Ce is the snow removal coefficient, Ct is the temperature condition coefficient, Pg is the weight of the snow layer on the horizontal projection of the ground, and C_s is the slope coefficient of the roof.

The ultimate limit state load combinations were applied according to Equation (6) [35].

$$D + 1.5L + 1.2(Lr \text{ or } S \text{ or } Rr) + 1.2(w \text{ or } 0.7E) \tag{6}$$

Where D is the dead load of the building, L is the live load on the floors, Lr is the live load on the arch, S is the snow load, Rr is the rain load, E is the design earthquake load, and w is the maximum wind load.

The foundation shear force caused by the earthquake refers to the sum of the lateral forces of the earthquake, which is applied to the foundation of the building according to Equation (7).

$$V = CW \tag{7}$$

Where V is the floor shear force and W is the effective seismic weight (including the dead load and the weight of facilities and infill walls as well as a percentage of the live and snow loads) [38-40].

The foundation shear force is distributed by the height of the building by Equation (8).

$$Fi = \frac{wh}{Wh} V \tag{8}$$

Where Fi is the lateral force at the level of the floor, w is the weight of the floor, including the weight of the arch and half of the weight of the walls and columns above and below the roof, and h is the height of the roof from the base level.

2.3 Shear resistance force of the wall [10]

The shear stress in 3D-printed structures can be defined as Equation (9) using Mohr–Coulomb theory.

$$\tau = \sigma \text{TAN}(\emptyset) + Cc \tag{9}$$

Where τ is the resistant shear stress in the wall, σ is the normal stress due to the weight of the upper layers, $\emptyset$ is the internal friction angle, and C_c is cohesion. The value of σ is calculated by Equation (10).

$$\sigma = \rho h \tag{10}$$

Where ρ is the concrete density, and h is the height of the wall.

To obtain the shear stress, the value of C_c should be determined by Equation (11).

$$C_c = \frac{(1 - \text{Ky}) + (1 + \text{Ky})\sin(\Phi)}{2\cos(\Phi)} \sigma \tag{11}$$

The value of Ky is equal to the Poisson ratio of the material.

2.3.1 The friction force [10]

The maximum frictional stress is obtained from Equation (12).

$$Fcr(i) = \frac{\mu V g}{Lbi} \tag{12}$$

Where $Fcr(i)$ is the maximum interlayer frictional stress, μ is the coefficient of internal friction, Vg is the gravity load caused by dead and live loads on the wall, L is the length of the multilayer beam or wall, and *bi* is the inner surface of the wall or multilayer beam.

2.4 FEA

The dynamic analysis of the structure under earthquake excitation was performed using the finite element software by introducing the ground displacement time history at the base level of the building. In this analysis, the damping ratio can be assumed to be 5%, unless it can be shown that other values are more suitable for the structure [40]. Currently, there is no consensus about how to select and scale the earthquake motions for code-based design and evaluation of the seismic performance of buildings using nonlinear response history analysis [41].

The finite element modeling of the 3D-printed structure was implemented using ABAQUS software following the criteria discussed in the National Building Regulations of Iran, Part 8 [36]. In the following, the loading of the structure

and the ultimate state load combination were defined. Tabas earthquake records were used as the design earthquake in this study. Finally, non-linear time history analysis of the structure was done, and the results were evaluated.

2.4.1 ABAQUS software [42]

ABAQUS is a commercial package for computer-aided FEA of structures. The Explicit solver is one of several multipurpose solvers in ABAQUS that uses the explicit integration method to solve problems with a high degree of nonlinearity, such as complex contact interactions and severe transient loads. In this study, the explicit solver of ABAQUS is used to analyze the considered 3D-printed building under seismic loads.

2.4.2 Material model

In the previous studies, no special constitutive model for 3DPC has been introduced yet [43]. According to past studies, the numerical simulation methods for masonry and other layered structures can be considered for 3DPC [44]. The material model used in this study was plain cement concrete (PCC) (not reinforced). Therefore, the Concrete Damage Plasticity (CDP) model was used to define the non-linear behavior of the material, which is available in the material library of ABAQUS. In order to obtain the inelastic behavior of the material, damaged elasticity, and isotropic tensile, and compressive plasticity can be used in the CDP

model. According to Equation (13), the total strain tensor ε consists of two elastic and plastic parts.

$$\varepsilon = \varepsilon_{el} + \varepsilon_{pl} \tag{13}$$

Where ε is the total strain tensor, ε_{el} is the strain tensor of the elastic region, and ε_{pl} is the plastic strain tensor.

In this model, isotropic hardening variables are expressed by inelastic compressive strain, cracking strain, including plastic hardening strain, and residual strain due to the damage. Hardening variables are used to control the crack development or failure level. Figure 2 shows the uniaxial compressive and tensile behaviors of the concrete material in the CDP model.

In Figure 2, σ_{cu} is the ultimate compressive strength, σ_{co} is the compressive strength, ε_{in} is the inelastic strain, and σ_c is the compressive strength of concrete. σ_t is the tensile stress, σ_{to} is the tensile strength, ε_p is the plastic strain tensor, and ε_t is the tensile strain. The compressive and tensile behavior of the unconfined concrete can be calculated based on the formulas presented in the literature [45].

Table 2 shows the specifications of the concrete material used in the 3D-printed structure model in this study. In this model, the results of previous studies on the behavior of unconfined plain concrete [45] have been used, which were assumed to be similar to the material behavior of the 3D-printed concrete considered here. In Table 2, f_{c0} is the initial uniaxial compressive yield stress, K is the shape parameter, and ρ is the mass density of the material.

(a) (b)
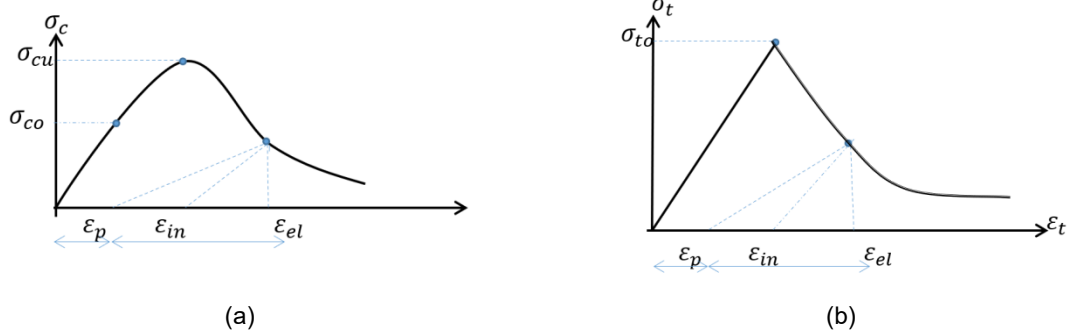
Figure 2. Concrete behavior: a) incompression; b) intension [45]

Table 2. Specifications of the concrete material model

Elasticity parameters		plasticity parameters	
Young's modulus(kg/cm^2)	250000	dilation angle (º)	30
f$_{c0}$	234	eccentricity	0.1
Poisson ratio	0.24	f$_{b0}$/f$_{c0}$	1.16
Friction coefficient	1.94	K	0.67
φ	20	viscosity parameter	0
		ρ (kg/m^3)	2100
compressive behavior		Compressive damage	
yield stress (kg/cm^2)	inelastic strain	damage parameter	inelastic strain
104.2	0	0	0
130.52	0.000077	0	0.000077
152.9	0.00017	0	0.00017
171.03	0.00028	0	0.00028
185.58	0.00042	0	0.00042

195.78	0.00057	0	0.00057
201.9	0.00074	0	0.00074
203.94	0.00093	0	0.00093
200	0.0011	0.01	0.0011
195	0.0013	0.04	0.0013
185	0.0016	0.09	0.0016
170	0.0018	0.16	0.0018
152	0.0021	0.25	0.0021
130.5	0.0024	0.36	0.0024
104	0.0028	0.49	0.0028
73.42	0.0031	0.64	0.0031
32.6	0.0035	0.81	0.0035
tensile behavior		tension damage	
yield stress (kg/cm^2)	cracking strain	damage parameter	cracking strain
20	0	0	0
0.02	0.00094	0.99	0.00094

Interfacial forces between the printed layers were introduced to the model using Equations (9)-(12). As mentioned before, each printing layer with a 4 cm thickness was subject to the bonding resistance of the face and the weight of the upper layers. FE modeling of the printing layers is illustrated in Figure 3.
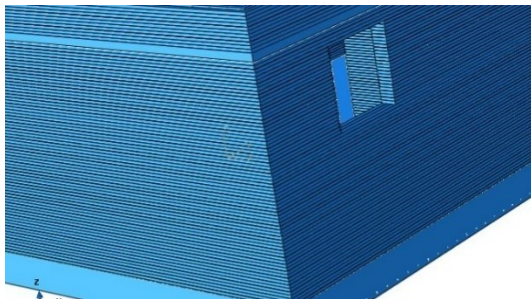
Figure 3. FE modeling of the consecutive printed layers

2.4.3 Boundary conditions and meshing

The nodes of the foundation floor were fully restrained against displacement and rotation in all directions. In the STEP of the earthquake excitation, the time history record of the earthquake was applied to the foundation nodes as boundary conditions (BCs). At the same time, the other degrees of freedom were still restrained. In order to avoid convergence problems in the software, three-dimensional HEX (8-node brick) elements with average dimensions of 30×30×30 cm were used to model the solid layers of the cross section. Also, the zigzagged grids between the two were modeled using 4-noded shell elements. Figure 4 shows the meshing of the FE model as well as the BCs defined in the analysis steps.

(a)

(b)

(c)
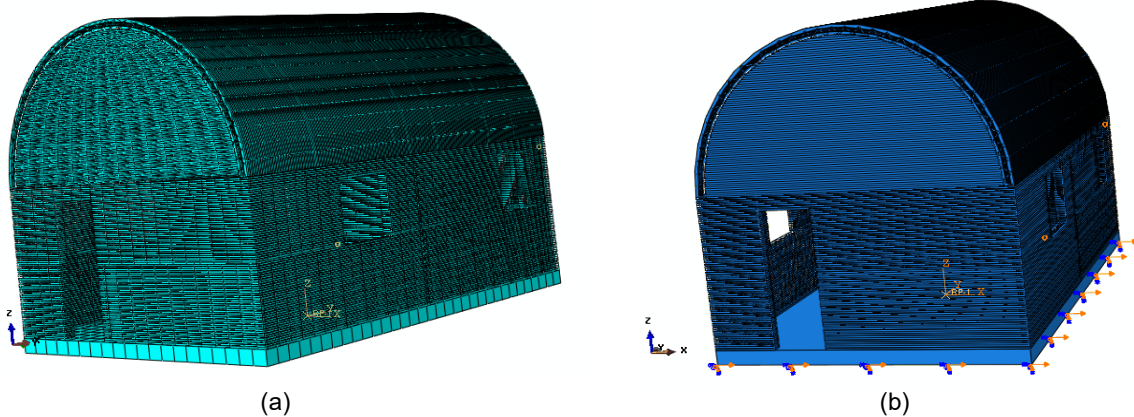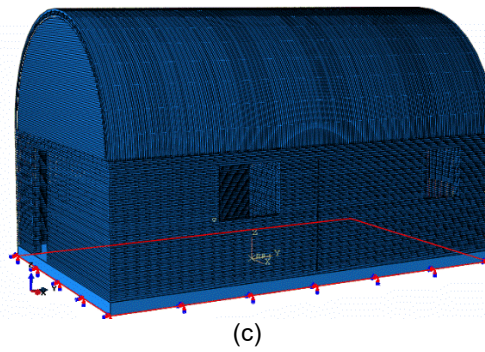
Figure 4. FE modeling of the considered building: a) meshing of the model; b) BCs for earthquake load step; c) BCs for initial and gravity load step.

In the analysis procedure of the model, a separate static general STEP was defined for gravity loads. A dynamic load STEP was assigned to the seismic loads as well, and the multi-step analysis was implemented. The results of the analyses were summarized and discussed in the following.

2.4.4 Seismic excitation

To put the earthquake loads on the building, the horizontal part of the earthquake accelerogram close to the Tabas fault, which has the details shown in Table 3 and Figure 5, was used. It came from a peer site [46]. Due to the time-consuming explicit analysis procedure in ABAQUS as well as the large number of elements in the considered model, only the records of severe ground motions from the earthquake were used here (Figure 6).

3 Results and Discussion

This section reviews the study findings regarding how seismic excitation affected the behavior of the 3D-printed structure. Here, the horizontal seismic excitation was applied once along the x-axis (transverse direction of the building) and the y-axis (longitudinal direction). The effects of external loading, cracks propagation, and the severity of damage to the structure during the earthquake were evaluated. In the following, the failure pattern of the structure was investigated. Finally, possible solutions to deal with the structural damages were presented according to the regulations and previous studies.

In this study, due to the lack of facilities to construct the 3D-printed structure as well as the lack of results of experimental studies on this type of structure, it was not possible to validate FEA results compared to the laboratory data. Hence, the results of all analyses were interpreted theoretically according to scientific principles and theoretical engineering considerations. Also, according to the design of the research model following the Iranian National Building Regulations, all the responses of the structure were controlled by those regulations.

FEA performed by Tahmasebinia et al. [47] on a model of a 3D-printed structure with arch roofing showed that the joints between the arch and walls and the foot of the arches were always the most critical positions under gravitational loads. These results are consistent with the results of the upcoming research. In the following parts, those results will be provided and discussed.

Table 3. Characteristics of the Tabas earthquake records

Spectral ordinate	event	year	station	Mag Mechanism
SRSS	Tabas,iran	1978	Bajestan	7.3
SRSS	Tabas,iran	1978	Boshrooyeh	7.3
SRSS	Tabas,iran	1978	Dayhook	7.3
SRSS	Tabas,iran	1978	Ferdows	7.3
SRSS	Tabas,iran	1978	Kashmar	7.3
SRSS	Tabas,iran	1978	Sedeh	7.3
SRSS	Tabas,iran	1978	tabas	7.3
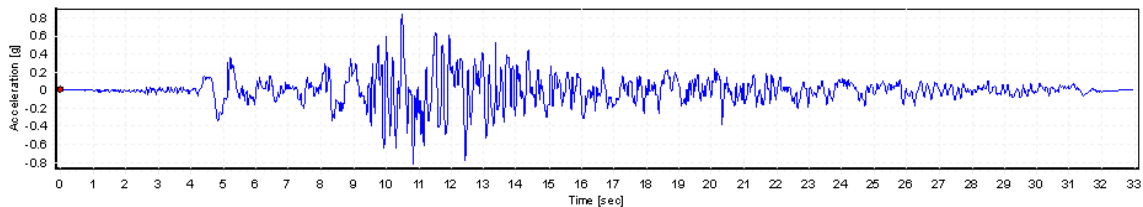
Figure 5. The Tabas earthquake accelerogram
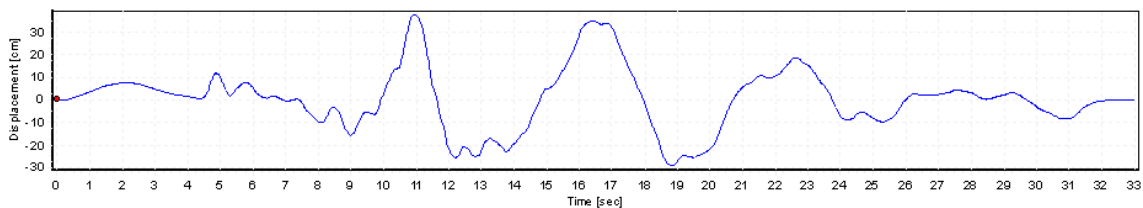
Figure 6. Strong ground movements of the Tabas earthquake records

3.1 Deformations and displacements

Figure 7 shows the structural elements before and after the seismic excitation along the x-axis (transverse direction of the building). Therefore, the undeformed shape of the elements is visible behind the deformed shape, as shown in Figure 7. The largest deformation occurred in the elements of the arch (the connection points to the wall) and in the connection points of the base of the walls to the foundation, where there is a sudden change in the geometry of the layers.

3.2 Deformation and stress in the arch system

Under seismic excitation along the x-axis, the von Mises stress quantities in the arch of the building along the path, as shown in Figure 8a, are drawn in Figure 8b. Due to symmetry in the structure and seismic excitation, only half of the arch span has been checked. Figure 8b shows that the von Mises stress has increased significantly in both halves of the arch. This result is rational because a shallow arch behaves like a beam under uniform loading conditions [48].

Figure 8c illustrates the variations in von Mises stress in the arch along the considered path in the z-direction (height of the structure). As shown in Figure 9c, the stress at the arc's beginning shows a higher value. But gradually, from the edge to the end of the first third of the arch, the stress reduces significantly. Then, in the middle third of the arch, a significant increase is observed again. Given that von Mises stress is used for normal, shear, and combined stress, as shown in Figure 8, it is concluded that the behavior of the arch corresponds to the behavior of a beam under a uniform load.

Figure 9a illustrates the variations in the displacement of the arch elements in the x-direction proportional to the distance along the arc, drawn along the same path as demonstrated in Figure 9a. The displacement shown in Figures 9a and b demonstrates that the failure occurred almost at the beginning of the arch. Also, the amount and trend of displacement in the x- and z-directions are very similar. So, at the beginning of the arc, the slope of displacement changes in the x-direction is much steeper than the displacement slope in the z-direction. This difference is due to the presence of a support in the z-direction. In the x direction, due to being in alignment with the lateral force as well as the gap space between the two faces of the truss section of the wall, higher displacement occurs.

(a)

(b)
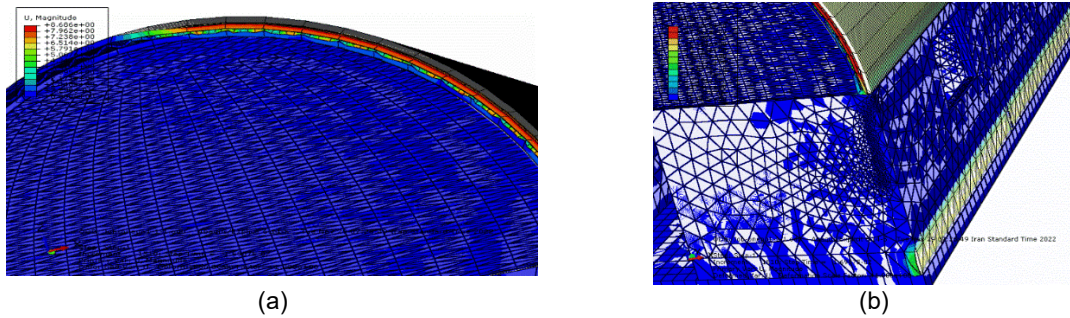
Figure 7. Deformed and undeformed elements of: a) thearch; b) thebody of the structure

(a)

(b)

(c)
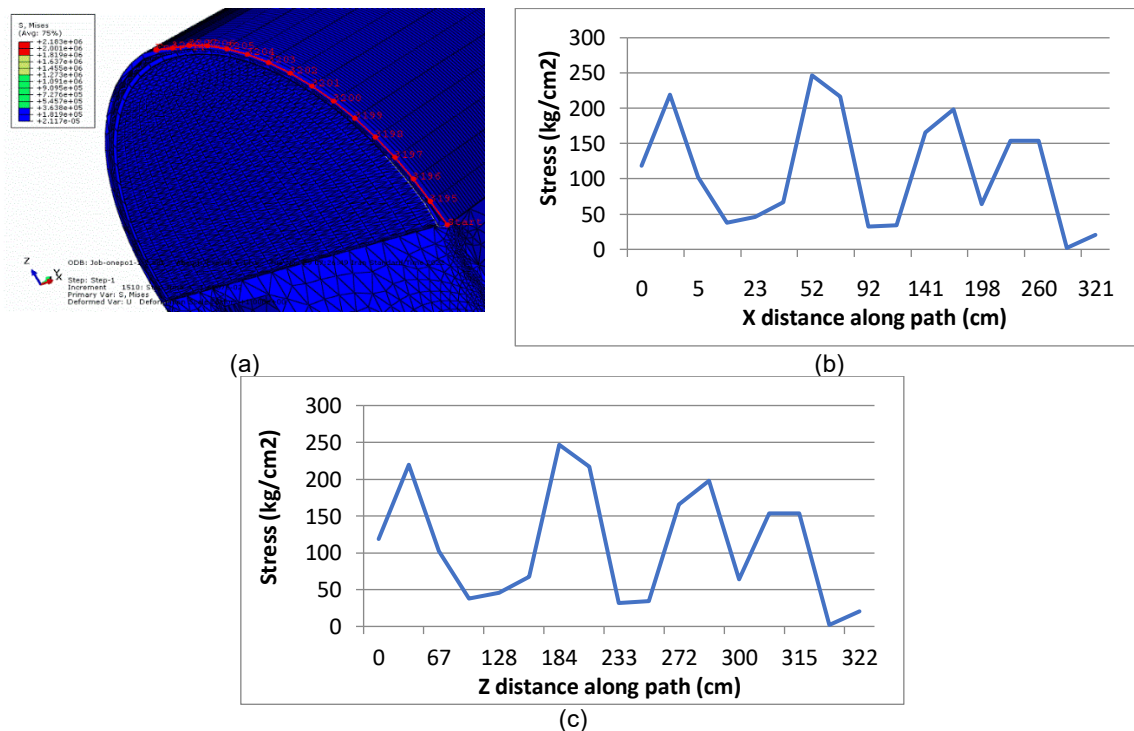
Figure 8. a) The considered path on the arch; b) von Mises stress variations in the x-direction; c) von Mises stress variations in the z-direction

(a)

(b)
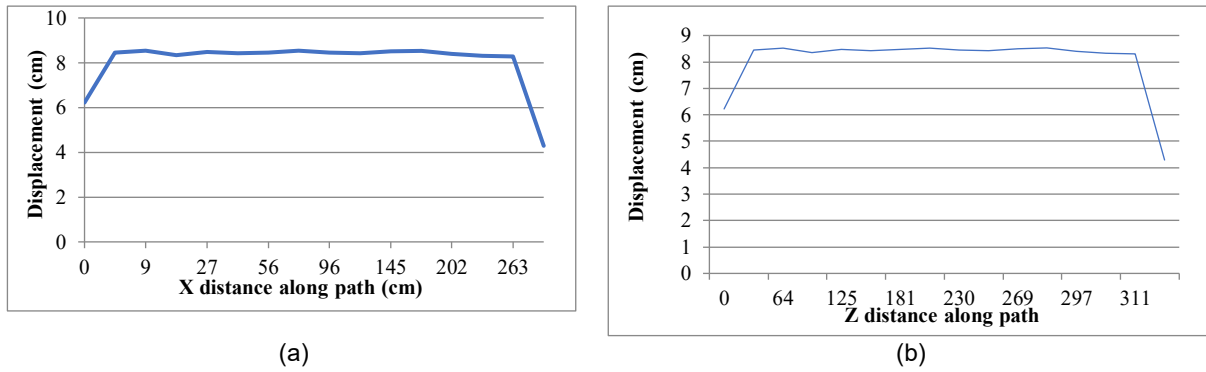
Figure 9. Displacement variations in the arch proportional to the distance from the beginning of the arch in the: a) x-direction; b) z-direction

By comparing Figures 8 and 9, it can be said that the stresses increase significantly in the middle of the arch. On the other hand, the high amount of displacement at the beginning of the arch has led to failure at this point. Therefore, at the beginning of the arch, i.e., at the connections of the arch and the wall of the building, there is a need to strengthen and/or replace the geometry or materials. In order to solve this problem, it is better to combine different arc radii in the arch or other roofing forms with a uniform change in the connection to the walls. In previous studies, other geometric shapes have been proposed for the roof of 3D-printed buildings [8, 49].

The maximum response value of the support reactions, as demonstrated in Figure 10a, is equal to 1.102×10^5 kgf (1.081×10^6 N). This was recorded in one of the middle nodes of the building's foundation, which has reached the point of yielding and failure in terms of resistance. On the other hand, the maximum plastic strain occurred in one of the middle nodes at the joint of the internal partition to the perimeter wall of the building (Figure 10b). The place where the maximum deformations occurred was on the edge of the partition wall connected to the perimeter wall. This reveals the critical effect of partition walls and their connection to the structure. Observations revealed that the highest stress in the structure occurred in the middle part of the longitudinal wall, perpendicular to seismic excitation. This point is precisely where the interior partition is connected to the perimeter wall of the building. Therefore, this also indicates the importance of placement and the existence of partitions in 3-D printed structures.

(a)

(b)

(c)
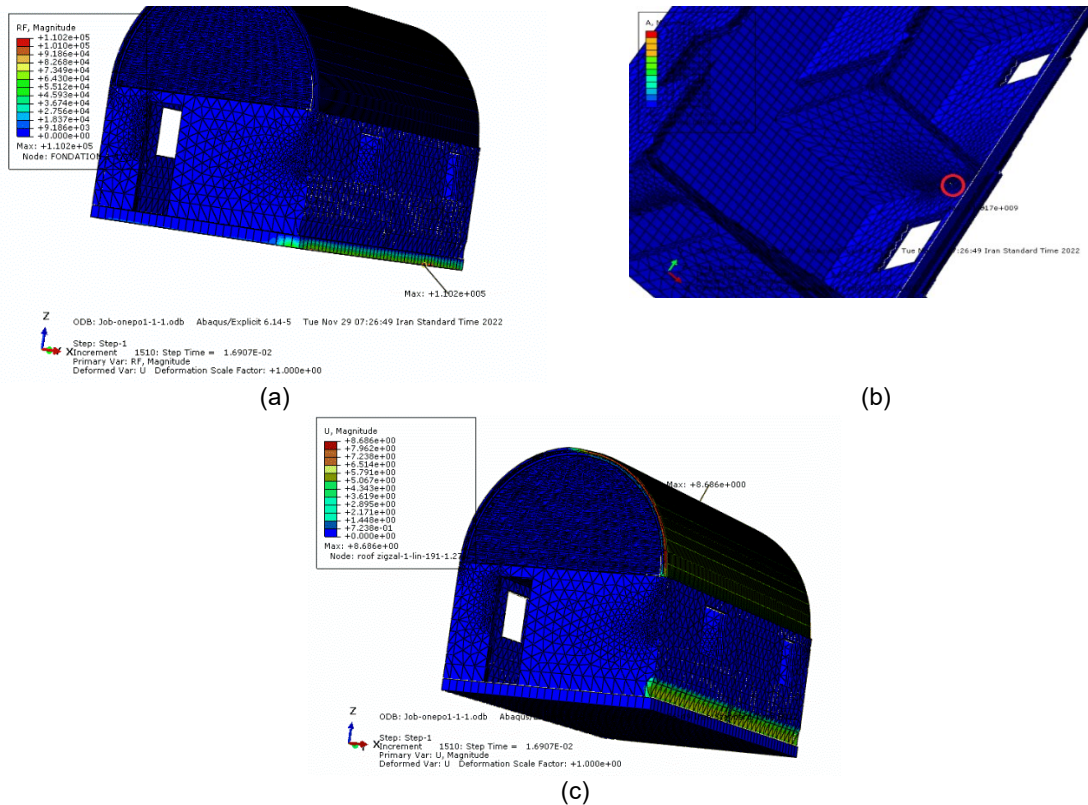
Figure 10. Extreme values of: a) support reactions; b) plastic strains; c) displacements

Figure 10c shows that the highest displacement in the structure is related to the grids located between the two layers of the arch. Most of the time, components of truss-like sections undergo buckling and instability issues before reaching the yield point. These large deformations cause structural collapse in the truss-like section components before reaching the yield condition. The walls of the model in this study also follow the pattern of truss behavior. In most cases, the arch is vulnerable due to the large displacement of the structure. This can be seen more clearly if the deformation is magnified, as shown in Figure 11.
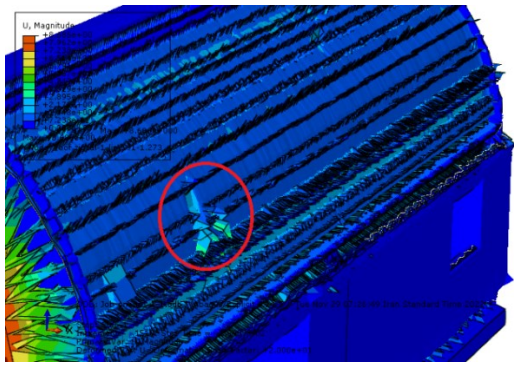
Figure 11. Maximum damage to the structure (magnified deformations)

3.2 Stress and displacement in the foundation

Under seismic excitation along the x-axis (transverse direction of the building), as shown in Figure 12a, a path was considered in the structure foundation in the direction of the y-axis for the changes in stress and reactions in the support (building foundation). Figures 12b, c, and d show the variations in von Mises stress, plastic strain, and support reaction forces in the considered path, respectively. Figure 11c shows that approximately 800 cm from the beginning of the path, along the length of the structure, the stress has the highest value. Also, at the beginning and end of the path, the amount of stress is found to be very large in the structure's foundation.

As shown in Figure 12d, the support force in the structure foundation near the distance of 800 centimeters from the beginning of the path has the highest value, as shown in the stress diagram. The presence of internal infill walls and their connection to the external walls on this side of the building can be the main cause of asymmetries in the stress and strain responses as well as the reactions in the foundation.

In the printing process of 3D structures, all the building components are executed layer by layer. Therefore, the partitions inside the building cannot be considered separately from the (lateral or gravitational) load-bearing system. This internal partitioning affects the behavior of the structure. Therefore, the thickness of the partition walls, their location, and their length are very significant issues.
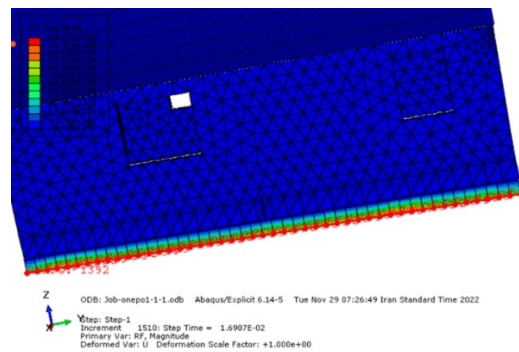
(a)
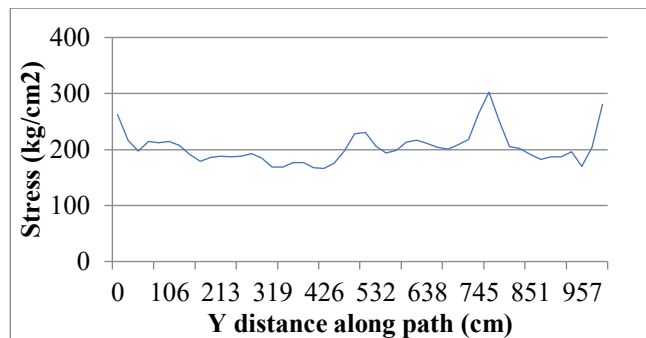
(b)
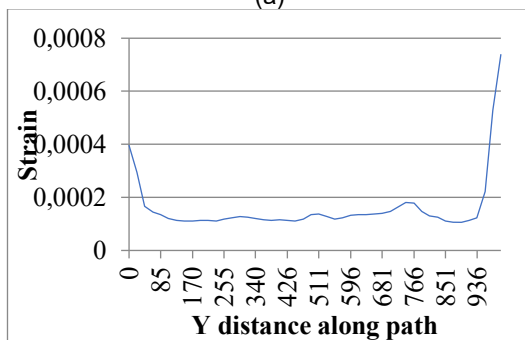
(c)
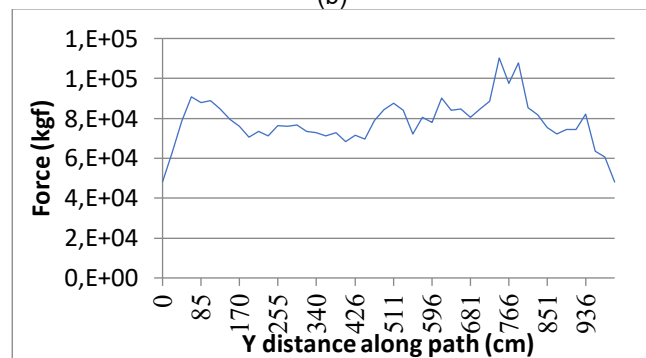
(d)

Figure 12. a) The considered path on the support; b) stress in the y direction; c) plastic strain, d) support reactions

3.3 Stress and displacement in the longitudinal direction of the structure

Under seismic excitation along the x-axis (the transverse direction of the building), Figure 13a shows the considered path in the arch. The diagram of the variations of the von Mises stress in the radial direction is drawn in Figure 13b. According to Figure 13b, in the middle part of the diagram, the value of the stress has reached zero in some elements. In the displacement diagram (Figure 13c), at the same point, the displacement response is at its peak value. As shown in Figure 13d, collapse has occurred at this point, indicating that failure (instability) has occurred due to large deformations. Therefore, it can be concluded that the structure needs to control displacement and strengthen the materials or sections used at the maximum displacement points.

It was observed that the highest base reaction was created at the beginning of the wall, i.e., at the connection zone of two external perpendicular walls. The reason for this is probably related to the shear behavior of the wall parallel to the direction of seismic excitation.

3.4 Seismic excitation in the longitudinal direction

In the case where the horizontal seismic excitation is defined along the y-axis (longitudinal direction of the building), as shown in Figure 14a, the damage to the roof of the structure is significant. Therefore, there are human life risks for the users of 3D-printed structures with truss-like sections. Therefore, if these structures are used in areas with very high seismic hazards, the necessary measures should be taken into account. As shown in Figure 14b, the roof of the structure has broken, and most of the zigzagged grids between the two layers of the arch are separated. As shown in Figure 14c, despite applying a high friction coefficient among the layers of the model, the sliding of the arch is evident on its supports. The sliding of the arch on the supports causes damage to the walls located in the inner part of the arch. Therefore, concentrated bending occurs in the arch, depending on the number of separating walls located in the internal parts of it.

(a)

(b)

(c)

(d)
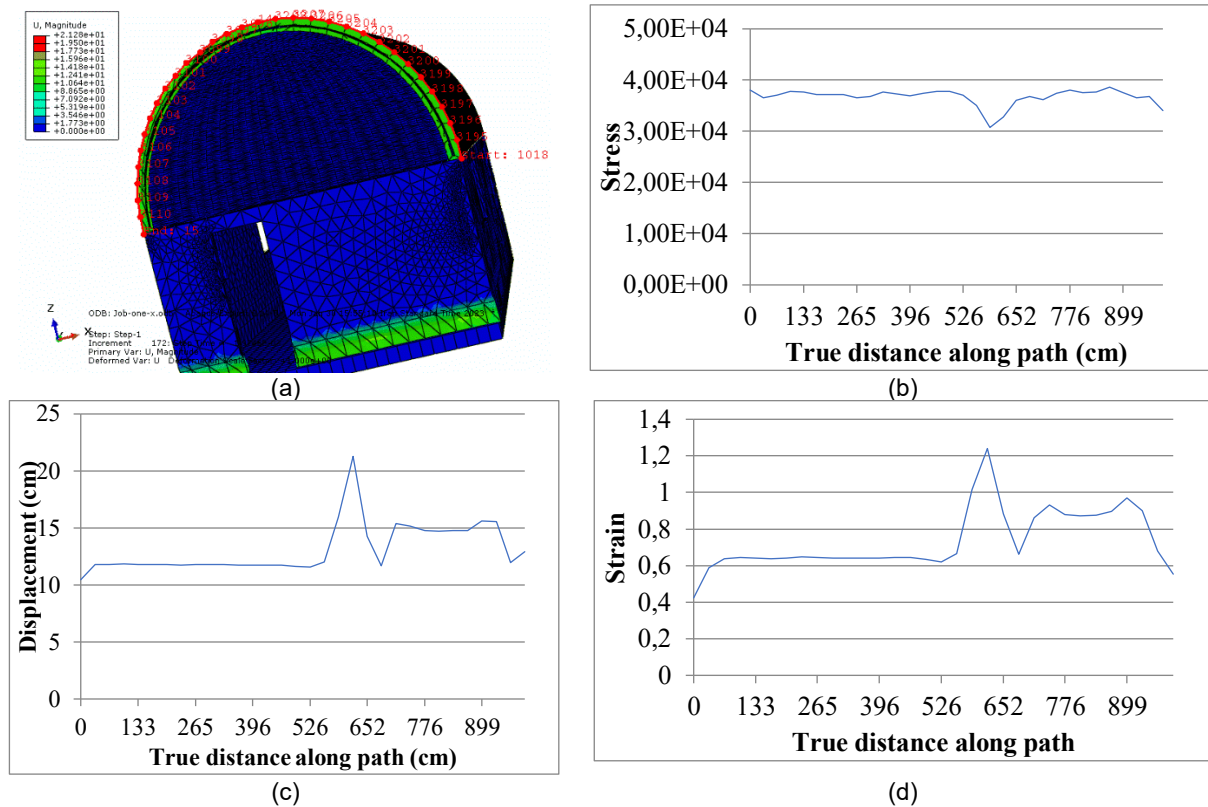
Figure 13. a) The considered path on the arch; b) von Mises stress; c) displacement; d) strain in the radial direction

(a)

(b)

(c)
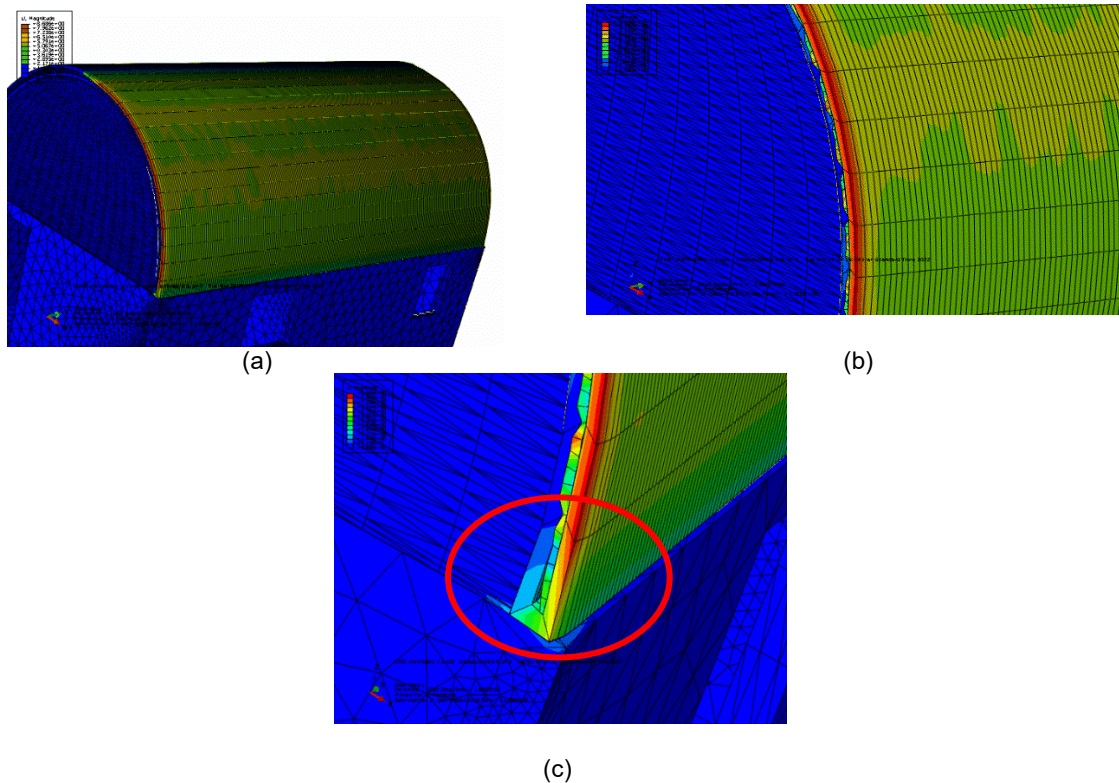
Figure 14. Seismic excitation on the length of the building, a. damage to the arch, b. damage to the grids between the windows, c. slipping of the arch over the living room

Adding rebars is one of the ways to increase the tensile strength and thus improve the behavior of the roof of 3D-printed buildings [15]. Although several studies have been conducted in this field, the practical application of this method requires complex technologies and expensive machinery, which leads to an increase in the total price of the printed structures. Another way is by adding fibers, especially long fibers, to the mixture of printing materials [14, 17]. It should be noted that excess use of those fibers can cause problems in the extrusion process. Therefore, some limitations should be considered when adding fibers to the mix [7].

Studies have shown that using smaller components and elements increases the load-bearing strength and reduces the stress concentration in 3DPC structures [1]. One of the cases that can improve the structural roof resistance is the reduction in the density of the concrete, which causes a lighter structure and thus reduces the seismic loads.

3.5 Shear force in the longitudinal direction

As shown in Figures 15a and b, the wall, which is considered the gravitational and lateral load-bearing system, is removed from the system, and the building faces complete collapse. Therefore, in the case of using this type of 3D-printed structure in areas with high and very high seismic risks, the necessary measures should be taken into account. For this purpose, the shear resistance of the walls should be increased, especially at the connection points to the foundation.

(a)

(b)
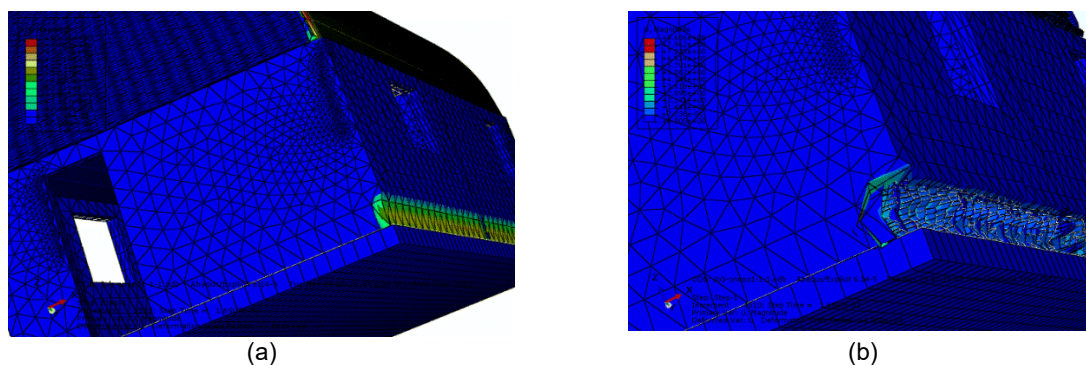
Figure 15. Shear damage to the foot of the walls under earthquake loading in the longitudinal direction of the structure: a) damage contours; b) magnified image of the wall'sdamage

One of the factors affecting the shear force applied to 3D-printed structures is the bond at the layer's interface. One of the critical solutions to the insufficient interface shear resistance is using steel rebars or fasteners [24]. As well, more suitable geometric shapes for the layers, for example, V-shaped forms that are placed inside each other, can be utilized [49]. Also, the design of short shear walls can be very effective.

4 Conclusion

Seismic safety is one of the basic needs of any structure located in an earthquake-prone environment. Printed structures are no exception to this rule. In this study, the behavior of a 3DPC building was investigated. The structure has a truss-like cross-section and is located in an area with very high relative risk. The Tabas earthquake records were selected as seismic excitations here. First, the basic needs of earthquake engineering for 3D-printed buildings were determined by extensive theoretical studies. Given the pilot nature of this study, a large part of the work included the same theoretical studies. Then, a prescriptive evaluation was done based on the regulations of similar structures. In the following, the safety methods of 3DPC buildings were discussed, and seismic evaluation was done using the results of explicit FEA by ABAQUS software.

According to the results, the displacement response played the most critical role in the structural failure. Most of the parts of the structure suffered damage and buckling due to local displacements before reaching the yield stress. The reason for this was the truss-like sections. In the state of seismic excitation along the length of the structure, tensile performance was dominant in the components. Due to the inherent weakness of concrete material in tension, the failure was higher than in the state where the seismic excitation was along the width of the structure. When the force of the earthquake was applied along the width of the structure, the arch roof of the structure had compressive behavior. The results of the analysis showed that the location of load-bearing and non-load-bearing walls (infill walls) was very significant. The presence of walls was very influential on the performance of the supports (building foundation). According to the results, the following can be suggested regarding the seismic behavior of 3DPC buildings:

− According to the hypotheses of this study, the structural components had a very low displacement and deformation capacity due to the functional properties of the materials. As a result, limiting and controlling displacements and rotations is a necessity.

− Using shear walls, 3D-printed structures can be secured against earthquake loads.

− Existing finite element software can be used to achieve a detailed and practical evaluation of 3D-printed structures to some extent.

For further studies and to complete this research, the authors decided to address materials with better tensile capacity and other types of 3D-printed structural models, such as printed buildings with limited human intervention under seismic loads.

References

[1] Pudjisuryadi, P., Antoni, A., & Chandra, J. (2020, September). Review on 3D printed concrete as structural beam members. In IOP Conference Series: Materials Science and Engineering (Vol. 930, No. 1, p. 012045). IOP Publishing.

[2] Schuldt, S. J., Jagoda, J. A., Hoisington, A. J., &Delorit, J. D. (2021). A systematic review and analysis of the viability of 3D-printed construction in remote environments. Automation in Construction, 125, 103642.

[3] Ahmed Saleh, A. E. (2019). 3D Printing in Architecture, Engineering and Construction (Concrete 3D printing). Engineering Research Journal, 162, 119-137.

[4] Allouzi, R., W. Al-Azhari, and R. Allouzi. (2020). Conventional construction and 3D printing: A comparison study on material cost in Jordan. Journal of Engineering.

[5] Mohammad, M., E. Masad, and S.G. Al-Ghamdi. (2020). 3D concrete printing sustainability: A comparative life cycle assessment of four construction method scenarios. Buildings, 10(12), p. 245.

[6] Jeong, H., Han, S. J., Choi, S. H., Lee, Y. J., Yi, S. T., & Kim, K. S. (2019). Rheological property criteria for buildable 3D printing concrete. Materials, 12(4), 657.

[7] Bohuchval, M., Sonebi, M., Amziane, S., & Perrot, A. (2019). Rheological properties of 3D printing concrete containing sisal fibres. Academic Journal of Civil Engineering, 37(2), 249-255.

[8] Khoshnevis, B. (2004). Automated construction by contour crafting—related robotics and information technologies. Autom. Constr,13, 5–19.

[9] Jagoda, J., Diggs-McGee, B., Kreiger, M., & Schuldt, S. (2020). The viability and simplicity of 3D-Printed construction: A military case study. Infrastructures, 5(4), 35.

[10] Suiker, A. S. J. (2018). Mechanical performance of wall structures in 3D printing processes: Theory, design tools and experiments. International Journal of Mechanical Sciences, 137, 145-170.

[11] Gebhard, L., Mata-Falcón, J., Anton, A., Dillenburger, B., & Kaufmann, W. (2021). Structural behaviour of 3D printed concrete beams with various reinforcement strategies. Engineering Structures, 240, 112380.

[12] Bukvić, O., Radonjanin, V., Malešev, M., & Laban, M. (2020). Basic fresh-state properties of extrusion-based 3D printed concrete. Građevinskimaterijali i konstrukcije, 63(4), 99-117.

[13] Van Zijl, G., Suvash, C. Suvash, C.P., Ming, J., Tan, M.J. (2016). Properties of 3D printable concrete. In Proceedings of the 2nd International Conference on Progress in Additive Manufacturing, Singapore.

[14] Li, Z., Hojati, M., Wu, Z., Piasente, J., Ashrafi, N., Duarte, J. P., Nazarian, S., Bilén, S. G., Memari, A. M. & Radlińska, A. (2020). Fresh and hardened properties of extrusion-based 3D-printed cementitious materials: A review. Sustainability, 12(14), 5628.

[15] Bos, F. P., Ahmed, Z. Y., Jutinov, E. R., & Salet, T. A. (2017). Experimental exploration of metal cable as reinforcement in 3D printed concrete. Materials, 10(11), 1314.

[16] Martens, P., Mathot, M., Bos, F., &Coenders, J. (2018). Optimising 3D printed concrete structures using topology optimisation. In High Tech Concrete: Where Technology and Engineering Meet: Proceedings of the 2017 fib Symposium, held in Maastricht, The Netherlands, June 12-14, 2017 (pp. 301-309). Springer International Publishing.

[17] Hojati, M., Nazarian, S., Duarte, J. P., Radlinska, A., Ashrafi, N., Craveiro, F., & Bilen, S. (2018). 3D printing of concrete: A continuous exploration of mix design and printing process. 42st International Association for Housing (IAHS).

[18] Tay, Y. W. D., Ting, G. H. A., Panda, B. I. R. A. N. C. H. I., He, L. E. W. E. I., & Tan, M. J. (2018, May). Bond strength of 3D printed concrete. In Proceedings of the International Conference on Progress in Additive Manufacturing, Singapore (pp. 14-17).

[19] Skibicki, S., M. Kaszyńska, and M. Techman. (2018). Maturity testing of 3D printing concrete with inert microfiller. in MATEC Web of Conferences. EDP Sciences.

[20] Phadnis, K., M. Shariff, and D. Menon. (2020). Optimal Rate of Printing of 3D Printed Concrete Columns and Walls to Avoid Buckling. in IOP Conference Series: Materials Science and Engineering. IOP Publishing.

[21] Federowicz, K., Kaszyńska, M., Zieliński, A., & Hoffmann, M. (2020). Effect of curing methods on shrinkage development in 3D-printed concrete. Materials, 13(11), 2590.

[22] Zainab, Olubukola. (2020). Exploring the Potential of 3D printing for Building Houses in Nigeria and Brief Numerical Analysis of Lintels in 3D Printed Houses. Graduate School of Science and Engineering Ritsumeikan University.

[23] Pekuss, R., A. Ančupane, and B.G. de Soto. (2021). Quantifying the complexity of 3D printed concrete elements. in ISARC. Proceedings of the International Symposium on Automation and Robotics in Construction. IAARC Publications.

[24] Wang, L., Ma, G., Liu, T., Buswell, R., & Li, Z. (2021). Interlayer reinforcement of 3D printed concrete by the in-process deposition of U-nails. Cement and Concrete Research, 148, 106535.

[25] Chang, Z., Xu, Y., Chen, Y., Gan, Y., Schlangen, E., & Šavija, B. (2021). A discrete 25 model for assessment of buildability performance of 3D-printed concrete. Computer-Aided Civil and Infrastructure Engineering, 36(5), 638-655.

[26] Licciardello, L., Reggia, A., Metelli, G., &Plizzari, G. A. (2021, November). Investigation of the Structural and Thermal Behaviour of 3D Printed Concrete Walls. In *Symposium on concrete and concrete structures* (pp. 18-19).

[27] Duarte, G., Brown, N., Memari, A., & Duarte, J. P. (2021). Learning from historical structures under compression for concrete 3D printing construction. Journal of Building Engineering, 43, 103009.

[28] Pan, T., Jiang, Y., He, H., Wang, Y., & Yin, K. (2021). Effect of structural build-up on interlayer bond strength of 3D printed cement mortars. Materials, 14(2), 236.

[29] Xiao J, Zou S, Yu Y et al. 3D recycled mortar printing: System development, process design, material properties and on-site printing. Journal of Building Engineering 2020; 32. https://doi.org/10.1016/j.jobe

[30] Xiao, J. Z., Liu, H. R., Ding, T., & Ma, G. W. (2021). 3D printed concrete components and structures: An overview. *Sustain. Struct*, *1*(000006), 10-54113.

[31] Es-sebyty, H., Igouzal, M., & Ferretti, E. (2022). Improving stability of an ecological 3D-printed house - a case study in Italy. *Journal of Achievements in Materials and Manufacturing Engineering*, *111*(1), 18-25.

[32] Zhang, D., Feng, P., Zhou, P., Xu, W., & Ma, G. (2023). 3D printed concrete walls reinforced with flexible FRP textile: Automatic construction, digital rebuilding, and seismic performance. *Engineering Structures*, *291*, 116488.

[33] Delavar, M. A., Chen, H., & Sideris, P. Design of 3D Printed Concrete Walls under In-Plane Seismic Loading. in 12th National Conference on Earthquake Engineering (12NCEE), Earthquake Engineering Research Institute (EERI), Salt Lake City, Utah, USA, 27 June – 1 July 2022.

[34] García-Alvarado, R., Moroni-Orellana, G., & Banda-Pérez, P. (2021). Architectural evaluation of 3D-printed buildings. *Buildings*, *11*(6), 254.

[35] Iranian National Building Codes Compilation Office (2020) INBC-Part 6: Structures Loading. Ministry of Housing and Urban Development (MHUD), Tehran, Iran.

[36] Iranian National Building Codes Compilation Office (2020) INBC-Part 8: Design and Construction of Masonry Buildings. Ministry of Housing and Urban Development (MHUD), Tehran, Iran.

[37] Iranian National Building Codes Compilation Office (2014) INBC-Part 9: Design and Construction of Reinforced Concrete Buildings. Ministry of Housing and Urban Development (MHUD), Tehran, Iran.

[38] Vice Presidency for Strategic Planning and Supervision, (2018). Instructions for Seismic Evaluation and Rehabilitation of Conventional Existing Masonry Buildings (Code No. 740). Tehran, Iran.

[39] Vice Presidency for Strategic Planning and Supervision, (2018). Instruction for Seismic Rehabilitation of Existing Buildings (Code No. 360), 1st Rev. Tehran, Iran.

[40] Building and Housing Research Center (BHRC). (2015). Iranian Code of Practice for Seismic Resistant Design of Buildings: Standard No. 2800-05, 4th Ed, Iran.

[41] Haselton, C. B., Whittaker, A. S., Hortacsu, A., Baker, J. W., Bray, J., & Grant, D. N. (2012, September). Selecting and scaling earthquake ground motions for performing response-history analyses. In Proceedings of the 15th world conference on earthquake engineering (pp. 4207-4217). Oakland, CA, USA: Earthquake Engineering Research Institute.

[42] Abaqus v. 6.14 Documentation; Dassault SystemesSimulia Corporation: Providence, RI, USA, 2014.

[43] Xiao, J., Liu, H., Ding, T. (2021). Finite element analysis on the anisotropic behavior of 3D printed concrete under compression and flexure. *Additive Manufacturing*, *39*, 101712.

[44] van den Heever, M., Bester, F., Kruger, J., & van Zijl, G. (2022). Numerical modelling strategies for reinforced 3D concrete printed elements. Additive Manufacturing, 50, 102569.

[45] Hafezolghorani, M., Hejazi, F., Vaghei, R., Jaafar, M. S. B., &Karimzade, K. (2017). Simplified damage plasticity model for concrete. Structural engineering international, 27(1), 68-78.

[46] Center for Engineering Strong Motion Data, CESMD. http://www.strongmotioncenter.org

[47] Tahmasebinia, F., Niemelä, M., EbrahimzadehSepasgozar, S. M., Lai, et al. (2018). Three-dimensional printing using recycled high-density polyethylene: Technological challenges and future directions for construction. Buildings, 8(11), 165.

[48] Dym, C.L. and H.E. Williams, Stress and displacement estimates for arches. Journal of structural engineering, 2011. 137(1): p. 49-58.

[49] Babafemi, A. J., Kolawole, J. T., Miah, M. J., Paul, S. C., & Panda, B. (2021). A concise review on interlayer bond strength in 3D concrete printing. Sustainability, 13(13), 7137.